ICRA2026 Late Breaking Results Poster presented at
2026 IEEE International Conference on Robotics and Automation (ICRA 2026)
June 1-5, 2026. Vienna, Austria

Vibration-Resilient LiDAR-Inertial Odometry with External Disturbance Compensation for Quadruped Robots

Quoc Hung Hoang, and Gon-Woo Kim, *Member, IEEE*

***Abstract*— This work presents a tightly coupled LiDAR–inertial odometry (LIO) framework tailored for quadruped robots operating under vibration and fluctuating conditions. By integrating time delay estimation (TDE) into an error-state Kalman filter (ESKF), external disturbances affecting the IMU are explicitly estimated and compensated during IMU pre-integration, significantly reducing vibration-induced errors. The resulting refined IMU poses are further used to correct LiDAR motion distortion, enabling a unified refinement process. This leads to smoother trajectories, improved localization accuracy, and enhanced robustness against both environmental and sensor uncertainties. The proposed framework is validated through real-time deployment on a quadruped robot.**

I. Introduction

Autonomous systems have seen significant progress across applications such as transportation, agriculture, logistics, and exploration. Among these, quadruped robots play an important role in tasks that demand accurate localization and reliable environment mapping. LIO enables high-quality 3D mapping; however, accurate pose estimation remains difficult due to uneven terrain and vibrations caused by locomotion, which amplify sensor noise. To address these challenges, IMU-derived motion can be utilized as feedback to compensate for motion-induced distortions in LiDAR measurements. Nevertheless, the high update frequency of the IMU also makes it more sensitive to noise, requiring effective suppression strategies. In this work, a sensor fusion framework for quadruped robots is developed that integrates LIO with external disturbance estimation and LiDAR distortion correction. An external uncertainty-aware TDE combined with an ESKF is employed to enhance trajectory stability. Experimental validation on a Unitree GO2 platform demonstrates that the proposed approach improves localization accuracy and produces smoother trajectories under dynamic operating conditions.

II. Proposed Method

First, the IMU measurement model is defined as follows:

$$\tilde{\boldsymbol{\omega}}_t = \boldsymbol{\omega}_t + b_t^{\boldsymbol{\omega}} + \boldsymbol{\eta}_t^{\boldsymbol{\omega}} + \boldsymbol{\varepsilon}_t^{\boldsymbol{\omega}} \tag{1}$$

$$\tilde{a}_t = a_t - R_B^W[\hat{q}_t](g) + b_t^a + \boldsymbol{\eta}_t^a + \boldsymbol{\varepsilon}_t^a \tag{2}$$

where $\tilde{\boldsymbol{\omega}}_t \in \mathbb{R}^3$ and $\tilde{a}_t \in \mathbb{R}^3$ are the measurement of the gyroscope and accelerometer in the IMU frame, respectively; $\boldsymbol{\omega}_t \in \mathbb{R}^3$ and $a_t \in \mathbb{R}^3$ are the true values of the angular velocity and acceleration, respectively; g is the gravity vector in world coordinates; The measurement of IMU is suffered from a slowly varying bias $b_t^{\boldsymbol{\omega}} \in \mathbb{R}^3, b_t^a \in \mathbb{R}^3$, additive white noises $\boldsymbol{\eta}_t^{\boldsymbol{\omega}} \in \mathbb{R}^3, \boldsymbol{\eta}_t^a \in \mathbb{R}^3$, and external disturbances $\boldsymbol{\varepsilon}_t^{\boldsymbol{\omega}} \in \mathbb{R}^3, \boldsymbol{\varepsilon}_t^a \in \mathbb{R}^3$; $R_B^W[\hat{q}_t] \in SO(3)$ is the rotation matrix from world frame to body frame.

The core idea of TDE is straightforward: when the time delay between two consecutive nodes in a factor graph optimization (FGO) is sufficiently small, the resulting uncertainty can be modeled as a continuous function, allowing the following approximation to be applied.

$$\hat{\boldsymbol{\varepsilon}}_t^{IMU} \triangleq \hat{\boldsymbol{\varepsilon}}_{t-\boldsymbol{\tau}}^{IMU} \tag{3}$$

The effect of white noise can be efficiently addressed using IMU preintegration [1], where it is incorporated into the covariance matrix during the optimization process. Consequently, it can be omitted from the noise terms in Eqs. (1) and (2). The remaining external uncertainty can then be expressed as follows:

$$\hat{\boldsymbol{\varepsilon}}_t^{\boldsymbol{\omega}} = \tilde{\boldsymbol{\omega}}_{t-\boldsymbol{\tau}} - \boldsymbol{\omega}_{t-\boldsymbol{\tau}} - \hat{b}_{t-\boldsymbol{\tau}}^{\boldsymbol{\omega}}; \hat{\boldsymbol{\varepsilon}}_t^a = \tilde{a}_{t-\boldsymbol{\tau}} - a_{t-\boldsymbol{\tau}} - \hat{b}_{t-\boldsymbol{\tau}}^a + R_B^W[\hat{q}_{t-\boldsymbol{\tau}}](g) \tag{4}$$

$$\hat{\boldsymbol{\varepsilon}}_{t-\boldsymbol{\tau}}^{\boldsymbol{\omega}} = \tilde{\boldsymbol{\omega}}_{t-2\boldsymbol{\tau}} - \boldsymbol{\omega}_{t-2\boldsymbol{\tau}} - \hat{b}_{t-2\boldsymbol{\tau}}^{\boldsymbol{\omega}}; \hat{\boldsymbol{\varepsilon}}_{t-\boldsymbol{\tau}}^a = \tilde{a}_{t-2\boldsymbol{\tau}} - a_{t-2\boldsymbol{\tau}} - \hat{b}_{t-2\boldsymbol{\tau}}^a + R_B^W[\hat{q}_{t-2\boldsymbol{\tau}}](g) \tag{5}$$

By substituting (4) into(5), the external uncertainty model can be derived as follows:

$$\hat{\boldsymbol{\varepsilon}}_t^{\boldsymbol{\omega}} = \tilde{\boldsymbol{\omega}}_{t-\boldsymbol{\tau}} - \hat{b}_{t-\boldsymbol{\tau}}^{\boldsymbol{\omega}} - \tilde{\boldsymbol{\omega}}_{t-2\boldsymbol{\tau}} + \hat{b}_{t-2\boldsymbol{\tau}}^{\boldsymbol{\omega}} + \hat{\boldsymbol{\varepsilon}}_{t-2\boldsymbol{\tau}}^{\boldsymbol{\omega}} + \frac{\left(\log\left(\Delta R_{t-\boldsymbol{\tau},t-2\boldsymbol{\tau}}\right)\right)\vee}{\boldsymbol{\tau}} + \boldsymbol{\mu}_t^{\boldsymbol{\omega}} \tag{6}$$

$$\begin{aligned}\hat{\boldsymbol{\varepsilon}}_t^a = {} & \tilde{a}_{t-\boldsymbol{\tau}} - \hat{b}_{t-\boldsymbol{\tau}}^a - \tilde{a}_{t-2\boldsymbol{\tau}} + \hat{b}_{t-2\boldsymbol{\tau}}^a + \hat{\boldsymbol{\varepsilon}}_{t-2\boldsymbol{\tau}}^a + \frac{\Delta v_{t-2\boldsymbol{\tau},t-\boldsymbol{\tau}}}{\boldsymbol{\tau}} \\ & + \left(R_B^W[\hat{q}_{t-\boldsymbol{\tau}}] - R_B^W[\hat{q}_{t-2\boldsymbol{\tau}}]\right)(g) + \boldsymbol{\mu}_t^a\end{aligned} \tag{7}$$

where $\Delta R_{t-\boldsymbol{\tau},t-2\boldsymbol{\tau}}$ and $\Delta v_{t-2\boldsymbol{\tau},t-\boldsymbol{\tau}}$ denote the IMU relative motion increments between two FGO nodes $t-\boldsymbol{\tau}$ and $t-2\boldsymbol{\tau}$; $\boldsymbol{\mu}_t^{\boldsymbol{\omega}} \in \mathbb{R}^3$ and $\boldsymbol{\mu}_t^a \in \mathbb{R}^3$ are the TDE errors; $(\bullet)\vee$ is the *vee* operator.

Subsequently, an ESKF is utilized to estimate the IMU orientation along with the external uncertainty of the quadruped robot. The corresponding ESKF formulation is provided in [2].

*This work was supported in part by Korea Innovation Foundation funded by the Ministry of Science and ICT in 2025. (No. RS-2025-02634783), and in part by the National Research Foundation (NRF) funded by the Korean government (MSIT) (RS-2024-00421129).

The authors are with the Intelligent Robotics Laboratory, Department of Intelligent Systems and Robotics, Chungbuk National University, Cheongju 28644, South Korea (e-mail: hoanghung950720@chungbuk.ac.kr; gwkim@cbnu.ac.kr).

Fig. 1. The configuration of the sensors.

In this study, the LOAM algorithm [3] is employed to estimate the LiDAR pose. A linear interpolation scheme is applied to mitigate motion-induced distortion in LiDAR scans by compensating for the sensor's relative motion within each scan, following the approach presented in [4].

Then, a factor graph is constructed to estimate the system states by jointly incorporating LiDAR odometry factors derived from LOAM and IMU factors.

III. Experiment Results

The proposed algorithm is validated in real time on a Unitree GO2 quadruped robot. The sensor suite comprises a 16-channel 3D Velodyne LiDAR, a MicroStrain 3DM-GX5-25 IMU, and a NovAtel PwrPak7D GNSS used for ground truth, as shown in Fig. 1. Experiments are conducted in a playground environment, which features sparse structural elements for LiDAR extraction and uneven terrain conditions. For comparison, other LIO approaches, such as LIO-SAM [4], are also included to further assess the effectiveness of the proposed method.

The comparative odometry results are presented in Fig. 2. Due to the irregular trajectory produced by conventional IMU preintegration, LIO-SAM applies compensation only for LiDAR rotational distortion in this scenario. While LIO-SAM demonstrates stable performance in the early stages, the estimated LiDAR trajectory still exhibits noticeable noise, as highlighted in the zoomed-in view. However, its pose estimation degrades during the third turn of the robot, primarily due to strong vibrations. In contrast, the proposed method successfully completes the trajectory with smoother odometry and achieves the highest accuracy, as reported in Table I. These results confirm that enhancing IMU preintegration is crucial for improving the overall performance of LiDAR–inertial odometry.

The disturbance estimation is illustrated in Fig. 3. The peaks in both acceleration and angular velocity occur periodically at intervals of approximately 0.5 seconds, corresponding to a frequency of around 2 Hz. This aligns with the robot's stomping pattern, which serves as the primary source of the observed vibration noise. To substantiate this claim, joint encoder measurements from all four legs are utilized as references for the robot's gait cycle. The peaks in the joint angles occur at the same frequency, showing strong agreement with the frequency estimated by TDE. This consistency suggests that the TDE-based noise estimation accurately reflects the true disturbance characteristics, indicating reliable performance.

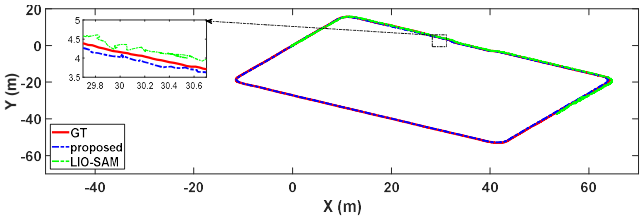

Fig. 2. Trajectories of the comparative methods.

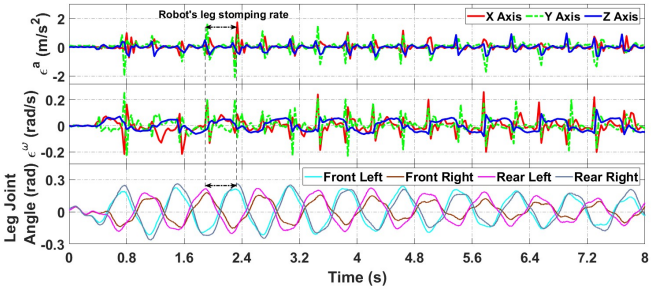

Fig. 3. ESKF response to external disturbances.

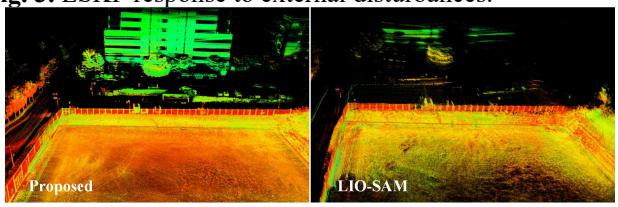

Fig. 4. Mapping performance for playground environment.

TABLE I
ERROR OF THE COMPARATIVE METHODS

Type	Translation error (m)	Rotation error (deg)	Running time (ms)
Proposed	**0.1742**	**0.425**	70
LIO-SAM	Fail	Fail	67

Figure 4 presents the mapping performance. Despite the environment consisting predominantly of ground-level features with limited structural elements, the proposed algorithm is able to reconstruct the scene effectively, demonstrating its robustness.

IV. Conclusion

In this study, the proposed algorithm incorporates uncertainty estimation for the IMU, thereby enhancing the performance of the SLAM system in highly uncertain environments and enabling successful deployment in an online application.

References

[1] C. Forster, L. Carlone, F. Dellaert, and D. Scaramuzza, "On-Manifold Preintegration for Real-Time Visual--Inertial Odometry," *IEEE Transactions on Robotics,* vol. 33, no. 1, pp. 1-21, 2017.

[2] Q. H. Hoang, and G. W. Kim, "IMU Augment Tightly Coupled Lidar-Visual-Inertial Odometry for Agricultural Environments," *IEEE Robotics and Automation Letters,* vol. 9, no. 10, pp. 8483-8490, 2024.

[3] J. Zhang, and S. Singh, "LOAM : Lidar Odometry and Mapping in real-time," *Robotics: Science and Systems Conference (RSS)*, pp. 109-111, 01/01, 2014.

[4] T. Shan, B. Englot, D. Meyers, W. Wang, C. Ratti, and D. Rus, "LIO-SAM: Tightly-coupled Lidar Inertial Odometry via Smoothing and Mapping." pp. 5135-5142.